ISBN: 978-3-95450-194-6 ISSN: 2226-0366 doi:10.18429/JACoW-LINAC2018-TU1A03

# STATUS AND ISSUES (MICROPHONICS, LFD, MPS) WITH TRIUMF ARIEL e-LINAC COMMISSIONING

S. R. Koscielniak†, T. Planche, S. Radel, Y. Ma, M. Alcorta, B. Humphries, F. Ames, E. Chapman, K. Fong, O. Kester, D. Kishi, R. Laxdal, M. Rowe, V. Verzilov, Z. Yao
TRIUMF, V6T 2A3, Vancouver, B.C., Canada

*Abstract*

The ARIEL electron linac (e-linac) is designed to generate cw beams of up to 30 MeV and 10 mA for delivery to a photo-convertor. Bremsstrahlung induced fission of a production target yields neutron-rich rare isotope beams to be supplied to the ISAC experimental facilities. The beam power will eventually reach 300 kW, and a machine protection system (MPS) with 10 μs rapidity is essential. The e-linac, which adopts 1.3 GHz, 2K SRF technology, is composed of a 10 MeV single-cavity injector cryomodule (EINJ) and a 20 MeV two-cavity accelerator cryomodule (EACA). The latter has vector-sum control of two cavities driven from a single klystron. Beam commissioning of these systems is ongoing since 2016. The magnetic optics and MPS commissioning to 10 MeV is reported herein. Beam has been accelerated up to 25 MeV, and threaded to the high energy dump (EHD). A campaign to investigate microphonics driving terms, LN2 disturbances, and a ponderomotive instability in the EACA, is underway.

## INTRODUCTION

The ARIEL* facility for rare isotope nuclear science was proposed in 2008 [1]. The facility and science program are described in [2, 3]. ARIEL-I Funding emerged in 2010, plans solidified in 2011 [4], leading to a mature linac design 2012 [5], construction of the EINJ in collaboration with VECC, Kolkota [6], and installation of EACA, with a single 9-cell cavity, was completed 2014.

Figure 1 shows the main sections of the e-linac and their naming. TRANSOPTR is adopted as the online beamline modeling and optimization tool [7] in the control room, and is used throughout the e-linac from source to beam dump.

Commissioning of the 300 keV low energy beam transport (ELBT/D) up to 1 kW beam power is reported in Refs. [7, 8]. Rudimentary beam tests on EINJ at 10 MeV and on EACA at 23 MeV each equipped with a single RF cavity were reported in 2014 [9] and 2015 [8], respectively. Preparation of the EACA for two-cavity operation is reported in [10, 11, 12, 13].

Throughout 2016 and 2017, attempts to commission the injector and medium energy transport were compromised by RF phase and amplitude jitter. Therefore, the 2018 campaign includes two objectives: commission magnetic optics, and identify (and abate) RF jitter sources. Further, by mutual agreement with the regulatory authority, e-linac operations at ≥ 10 MeV are not permitted above 100 W beam power until the machine protection is commissioned.

## ELECTRON GUN

Operation of the thermionic electron gun (EGUN) is reported in Ref. [14]. Performance of the gun itself has been excellent. After overhaul of the high-voltage power supply by Glassman in 2016, the HVPS has also proven reliable.

For >10 MeV commissioning it is critical that the EGUN supports a duty factor ranging from 0.01% to cw so that beamline components are subjected to low average power during beam threading if there is accidental beam loss.

### *Stable Duty Factor Parameters*

The HVPS is nominally a DC supply, but we pulse it. Stable combinations of repetition rate and pulse length have been measured. At 100 μA peak, the combinations of 50 Hz to 10 kHz and 5-200 μs are stable. At 10 mA, the combinations 100 Hz to 2 kHz and 5-50 μs are verified stable duty factors [15].

### *Measured Beam Energy Stability*

Results from ELBD with high-dispersion optics confirm the energy stability of the HVPS at 0.01%. Contrastingly, the sum signal from the first beam position monitor (BPM) after the gun show a 60 Hz phase jitter ~ 0.2° at 650 MHz.

## OPTICS COMMISSIONING

### *Polarity Check*

Prior to beam tests, the polarity of every magnetic element was checked using a Hall probe. This proved to be a worthwhile time saver as the polarity of several steerers and quadrupoles was found to be incorrect.

### *Optics Commissioning with Beam*

Beam commissioning began at very low average power (< 10 W). All magnetic elements were tested individually:

- Steerers by their effect at downstream beam position monitors (BPM).
- Quadrupoles by searching for the setting which achieves minimum beam size on a fluorescent screen, and by comparing this setting with our optics model.

All magnetic elements performed precisely as expected.

### *RF Commissioning with Beam*

The injector optics design is given in Ref. [16]. The gun emits 650 MHz bunches; these are energy modulated, head-to-tail, by a 1.3 GHz buncher cavity [6] to prepare them for the EINJ 9-cell cavity acceptance at 300 keV.

* ARIEL is funded by the Canada Foundation for Innovation, the Provinces AB, BC, MA, ON, QC, and TRIUMF. TRIUMF receives funding via a contribution agreement with the National Research Council of Canada.
† shane@triumf.ca.

ISBN: 978-3-95450-194-6 ISSN: 2226-0366 doi:10.18429/JACoW-LINAC2018-TU1A03

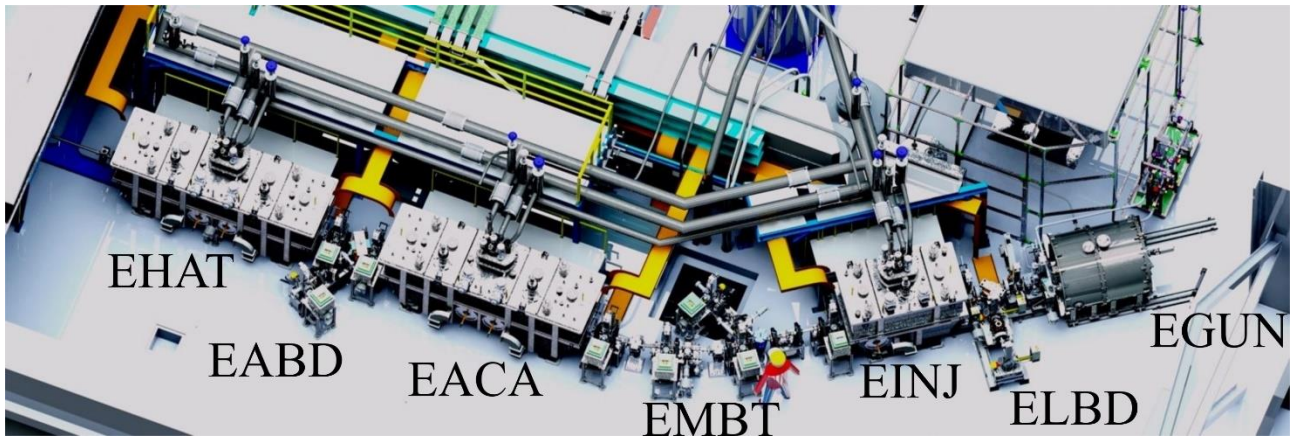


Figure 1: Rendering of the e-linac. The future, cryomodule EACB is presently replaced by the EHAT beam transport.

The three SRF cavities were initially commissioned without bunching. The accelerated beam energy was measured at an analyzer dipole magnet, and the cavity phase set to achieve maximum energy gain.

The RF buncher was then phased to minimize the energy spread downstream of EINJ as inferred from the beam profile on a fluorescent screen at a dispersive location. The buncher amplitude was determined by minimizing the beam loss monitors readings. Transmission down all beamline sections was, within the few percent accuracy of our Faraday cups, 100%. Note, when properly set, variation of the buncher phase and amplitude has little impact on the beam position, although it alters the horizontal beam size, as a consequence of energy spread.

### *Tune Development*

Steerers were adjusted such that each quadrupole would not steer. This was verified by varying each quadrupole while looking at downstream BPMs. The doubly achromatic EMBT bend section was tested by varying together dipoles at both ends, while making sure that the beam does not move on any of the downstream BPMs.

### *Medium Energy Beam Transport*

The EMBT optics design (magnets & diagnostics) is given in Ref. [17]. Our overall understanding of the optics was tested by measuring the RMS size of the beam along the beamline, and comparing it to our linear optics model (see Fig. 2). The actual settings for quadrupoles differ from theoretical values by less than 0.5%.

### *EABT/D & EHAT Beamlines*

The accelerated beam optics design, EACA to EABT to EHAT, is described in Ref. [17]. Nominally, the EACA output is 30 MeV, but is limited by the Ponderomotive instability to 25 MeV. Failure of one of the three sub-atmospheric pumps further reduced the output beam to 22 MeV. EABT consists of three weak quadrupoles (like those upstream), two steerers, three BPMs and view screen (VS). Between the first two quadrupoles a dipole can bend the beam into the EABD section with two weak quadrupoles,

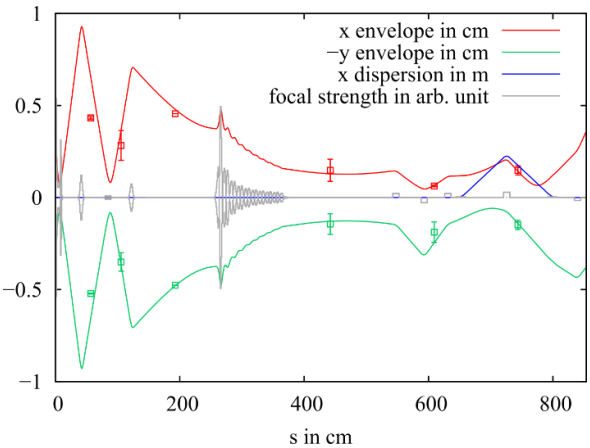


Figure 2: Beam envelope along ELBT and EMBT calculated by TRANSOPTR (solid lines) compared to measured 2 r.m.s beam sizes (square dots). The error bars reflect the sensitivity of the r.m.s value to the background cut.

two steerers and one screen in front of the dump, a Faraday cup. The EABD quadrupoles were used to increase the dispersion in x to observe the beam energy instability from EACA on the view screen.

The EHAT beamline consists mainly of a long drift where the future cryomodule EACB is placed, four medium quadrupoles (with stronger focussing strength), three steerers and three beam position monitors.

The functionality of all quadrupoles was verified, as well as all steerers. All optic elements in EABT/D and EHAT work as expected. For the commissioning all quadrupoles in EABT and EHAT were turned off. Thus, these beamlines acted as a very long drift as depicted in Fig. 3.

### *EHDT Beamline & Dump*

Beam transport (magnets & diagnostics) to the dump is specified in Ref. [18]. The EHDT beamline is not commissioned. A 3 W beam was sent to the EHD dump. The fact that we can form a sharp beam image, Fig. 4, of the cathode and that it is free of distortions illustrates that overall the transverse optics is very linear.

ISBN: 978-3-95450-194-6 ISSN: 2226-0366 doi:10.18429/JACoW-LINAC2018-TU1A03

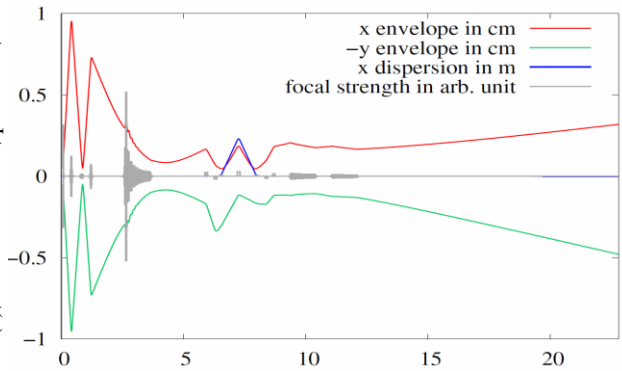


Figure 3: Beam envelope along ELBT, EMBT, EACA, EABT and EHAT calculated by TRANSOPTR.

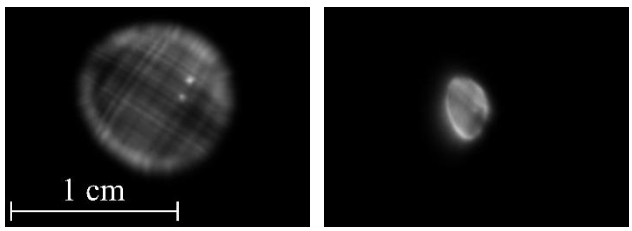


Figure 4: Left: beam spot object on ELBT:VS2. Right: beam spot image at EHDT:VS4.

The core of the EHD tuning dump [19, 20] is an inclined plane of Al alloy with water cooling on the back surface. The dump is rated for 100 kW with beam spot scanning and 10 kW without. Cooling circuits, temperature sensors and interlocks, including FSD interface, are all functional.

## CONTROLS

In the interest of control systems reliability, several incremental improvements were made: modifications to view-screen IOCs, updating support packages for the beam positions monitors, and expanding Beam Modes (allowed combinations of beam path and beam power) logic to include paths beyond EACA to EHD.

When a beam mode is granted, the magnetic benders on that beam path are restricted to ±1% about the excitation current calculated from beam energy.

An extensive package has been written to interface the TRIUMF-designed beam loss monitor data acquisition boards to the EPICS support of the overall MPS.

### *Optics Lock*

The most recent and significant advance is the introduction of the Optics Lock (OL) as part of the Beam Modes. OL facilitates the transition from tuning to operation. The changing of magnetic optics and RF cavity set points is only permitted below 100 W beam power. With the exception of the duty factor, the equipment set points must be locked before the power can be raised above 100 W.

## MACHINE PROTECTION SYSTEM (MPS)

The MPS must have rapidity (trip < 10 μs) to respond to full beam loss and large dynamic range (> $10^4$) to detect the onset of beam loss. System has three layers of protection: (1) interlocks, (2) trip on beam position, (3) trip on beam loss. All trips are implemented by the Fast Shut Down (FSD). Commissioning of the ELBT/D MPS which uses photo-multiplier tubes (PMTs) and a JLab-supplied electronics board was reported in Ref. [7]. The downstream beamlines use long ionization chambers (LICs) as the backbone BLMs, supplemented by PMTs in shadowed locations. Since 2016, TRIUMF has developed its own more versatile integration and threshold electronics board [21, 22] and deployed in EMBT/D and beyond.

### *Beam Position & Loss Monitors (BPM & BLM)*

Each BPM consists of 4 buttons, and measures horizontal and vertical beam offset for display in the control room. Firmware on the 100 MHz data acquisition boards monitors the beam position; if it exceeds prescribed limits then a beam trip request is send to the FSD on an optical fibre link. The BPM MPS layer is complete to the EHDT dump.

Two types of loss monitor are used: scintillators, consisting of a small BGO crystal coupled to a PMT; and LICs filled with a flow of Argon gas for prompt charge collection. Both BLM types have proven a range of $10^6$, from 100 pA to 100 mA.

### *BLM Electronics Board (TBLM)*

The BLMs are connected directly to the TRIUMF electronics boards (TBLM) which integrates incoming signals, and sends a trip via fibre-optic to the FSD upon exceeding a pre-determined threshold. The hardware integration time is set to 100 ms with a total charge of 1 nC. An ADC samples the output of the integrator at 1 MHz, so that a continuous difference calculation is available every 1 μs.

The trip is defined by either of two conditions: a "delta" trip (for large/fast losses) and a "100 ms" trip (for lower/slower losses) each with a configurable threshold. The "delta" trip occurs when a single difference value is above a configurable threshold. The "100ms" trip uses a sliding window integration: $10^5$ consecutive readings summed.

### *EMBT/D and EABT/D & EHAT*

The BLM aspect of the EMBT/D MPS has recently been commissioned up to 100 W and 10 MeV. Four BLMs are used to ensure total coverage of this section: three LICs and one PMT. The LICs are positioned to include redundancy in most areas of the beamline, while the PMT is placed at the dipole magnet leading to EMBD to detect spills inside the magnet. Commissioning took place over two weeks and consisted of first performing beam spills to determine optimal numbers of BLMs and their locations, and then a final step which included purposeful beam spills above threshold to ensure a trip of the e-gun takes place within the specifications. The controlled spills were performed at low duty factors using a combination of quadrupoles and steerers to mimic point losses in both planes (H & V) of the beamline.

Commissioning the beamlines immediately downstream of EACA is ongoing. The total number and type of BLM has not yet been finalized, but it is likely to include six LICs and at least two PMTs (placed to detect losses inside dipole magnets).

ISBN: 978-3-95450-194-6 ISSN: 2226-0366 doi:10.18429/JACoW-LINAC2018-TU1A03

### *Dark Current Effects*

Above a gradient ≈ 9 MV/m per cavity, the EINJ and EACA cavities both produce dark currents significant enough to compromise the BLMs. The currents are seen on view screens upstream and downstream of the cavities and found to extend up to 4.5 MeV.

### *MPS Outlook & Future Developments*

The TBLM board stores up to 1 s of data in memory. All data is frozen at the trip condition, and can be interrogated via the EPICS interface. This will allow the beam operators to visualize the post mortem waveform for each BLM, synchronized in time, to determine where a loss took place and troubleshoot the cause of the spill.

## RF REGULATION & INSTABILITY

Synchronization of the radio frequency (RF) with the electron beam is critical to acceleration. The combination of narrow electrical bandwith of SRF cavities and the high oscillation frequency (1.3 GHz) makes acceleration very sensitive to phase and amplitude jitter. The possible causes of jitter are: RF source master oscillator, external disturbances, microphonics, ponderomotive instability, and the inability of the RF control loops to supress the effect of these disturbances; all have been observed in the e-linac.

The best probe of jitter effects is the electron beam itself, particularly downstream of bending magnets – whose effect is sensitive to momentum. Some RF measurement devices perform averaging due to their inherent time constants, and so fail to report meaningful values for phase and/or amplitude noise. Contrarily, r.m.s and peak-to-peak variations are easily seen on beam diagnostic devices such as BPMs or view screens [23]. However, stroboscopic effects can mask the underlying frequencies.

### *Microphonic versus Ponderomotive*

Cavity mechanical modes can respond both to external acoustic noise and to internal electro-magnetic pressure; respectively called the microphonic and ponderomotive effects. Both can lead to changes in the cavity electrical resonance frequency. They differ in that above a threshold accelerating gradient, the ponderomotive effect [24, 25] can be self-enhancing leading to an exponential and/or oscillatory instability of all system signals. A microphonic detuning can act as the seed for instability.

### *Master Oscillator (MO)*

Significant phase drift and jitter between the EGUN, buncher and EINJ were witnessed in 2016, and a program of upgrades to the MO and LLRF were performed in 2017. Originally four MOs were used, 1 for each RF device, and synchronized by a 10 MHz clock. Now, there is a single MO signal split between the devices; stability is excellent.

### *Injector & Accelerator Cryomodules*

Design and construction of EINJ is described in Ref. [26]. EINJ is a top-loading cryomodule. 2 K liquid helium is produced on board via a Joule-Thomson (JT) expansion of externally supplied 4 K LHe. The assembly is enclosed in a LN2-cooled thermal shield. The cold mass comprises a strong back, cavity and scissor-type tuner. The tuner is actuated by a stepper motor at room temperature via rods that pass through the lid and shield. The cavity is driven via two Cornell-type coaxial couplers; each is rated at 50 kW and cooled by compressed air.

At the outset of the 2018 commissioning, momentum jitter of ~ 0.5% was observed at the exit of EINJ. Adjustments in phase set points and tuning of LLRF control loop parameters has reduced this to $\Delta p/p \sim 0.1\%$.

The 0.1% level $\Delta p/p$ is tolerable, but not conducive to easy/fast tuning of correction bends in EMBT/D. Therefore, a campaign to investigate underlying causes was begun; starting with a frequency analysis of the cavity pick-up signal versus the master oscillator. A strong and persistent 40 Hz sideband, among other frequencies, gave cause to initiate a campaign of diagnosing microphonic sources and effects in EINJ and EACA.

Design and construction of EACA, which adopts features from the EINJ, is described in [26]. EACA operated with a single cavity in 2014 and 2016. The second EACA cavity was installed in 2017 but not operated. The two cavities are driven from a single klystron through a power divider. In addition to microphonic effects similar to those in EINJ, operation of EACA in 2018 revealed an oscillatory ponderomotive instability occurring at positive detuning and threshold gradient of ~ 6 MV/m per cavity. This discovery initiated measurements of the Lorentz Force Detuning (LFD) characteristics of the cavities, theoretical analysis and simulation of LFD instability.

## MICROPHONICS INVESTIGATION

If a peak in the acoustic noise spectrum lies within the bandwidth of a mechanical mode of the cavity, then oscillations will alter the cavity electrical resonance frequency.

### *Cavity Mechanical Normal Modes*

The low order transverse and longitudinal mechanical modes of the 9-cell cavities have been computed [27] with 3D modelling software. The presence of the coupler ports splits the transverse modes. The 3D model has limitations. An attempt to verify the mode frequencies has been made with a swept-frequency external shaker. The shaker does not couple equally well to all modes, but confirms the fundamental and first three harmonic transverse oscillations.

### *Acoustic Noise Sources*

Comprehensive measurements of noise sources, including turning equipment on/off or throttling, have been made leading to the identification of sources, locations, frequency spectra, and transmission through ground, plumbing, waveguides, RF input couplers, etc. The main sources:

- Water cooling systems for klystrons & waveguides: multiples of 60 Hz up to 420 Hz; and sum/diff 30 Hz satellites. The 60 and 300 Hz lines are very strong.
- On-board Joule-Thomson valves (act like blown pipe), particularly for EINJ. Strong components at 40, 80 Hz

ISBN: 978-3-95450-194-6 ISSN: 2226-0366 doi:10.18429/JACoW-LINAC2018-TU1A03



- Air cooling for RF input couplers; line around 200 Hz and strong noise above 300 Hz.
- Cryomodule roughing pump vacuum lines: transmit 30, 60, 120, 180, 220 Hz.

Example measurements are shown Ref. [27] Fig. 3. The GHe and LHe plant and trunk seem not to be noise sources.

### *Response of Cavities to Microphonics*

The response to microphonics has been measured using cavity pick-up signals and phase error within the LLRF, and with a variety of instruments. The most successful has been the Phase Analyzer on loan from Rhode & Schwarz. This has requisite resolution and sensitivity, and automatically orders spectral lines according to impact. A 1:1 correspondence between noise sources and RF phase modulations based on their frequency spectra. E.G. the EINJ spectra and noise source identification is given in Ref. [27] Fig. 2. The spectra show also a non-acoustic source: lines at multiples of 60 Hz from 480 to 900 Hz emanate from the klystron DC high voltage switch-mode power supply; these lines are inconsequential.

### *Liquid Nitrogen Disturbances*

The cryomodule LN2 supply valve is controlled by exhaust temperature, and poorly regulated. This leads to LN2 & temperature bursts & RF power fluctuations all with period 500 secs. Moreover refilling the LN2 reservoir/phase-separator leads to transients twice/hour. Both effects can exceed the microphonic sources. See Ref. [27] Figs. 8-10.

### *Proposed Mitigations*

Water cooling pumps and piping system will be acoustically damped, as will be the RF waveguides. The acoustic property of the 4K/2K LHe insert including JT valves will be examined. A non-intermittent regulation of the LN2 supply will be implemented.

## PONDEROMOTIVE INVESTIGATION

The e-linac SRF cavities are operated in self-excited (SE) loop. The EINJ has been operated in four years, and never displayed an instability. The EACA was operated for the first time with two cavities regulated in vector sum, in June 2018. An instability emerges when the combined accelerating gradient of EACA cavities exceeds 12 MV/m. Properties of the instability include the following:

- Thresholding
- Modulation of cavity amplitudes in-antiphase
- Frequency around 160 Hz, but varies with parameters
- Slow growth: over minutes at 12 MeV, secs at 17 MeV
- Final amplitude limited by klystron forward power
- Growth rate rises with accelerating gradient
- Sensitive to individual cavity detunings.
- In-phase AM if the cavities are grossly mis-phased.

See Ref. [27] Fig.1. Investigation and explanation of the instability is progressing on three fronts. [Previous analysis [28] of vector sum control revealed sensitivity, but not instability.]

### *Lorentz Force Detuning Measurements*

LFD changes the response of cavity mechanical modes to acoustic noise, and is the foundation for understanding how the ponderomotive instability arises and is influenced by RF distribution and control loops. Dynamic LFD is used as an input to ponderomotive simulations.

Steady State or Static LFD: the cavity fundamental resonance frequency falls proportional to gradient squared.

In the dynamic LFD measurement, the carrier is amplitude modulated (AM) at a certain frequency. Cavity mechanical modes near that frequency respond, leading to detuning. The phase difference between drive and pickup is used as proxy for the frequency detuning. LFD measurements on EINJ and EACA single cavities have been performed at frequencies (20 – 300 Hz) found to be important with the R&S phase analyzer; an example is given Fig. 5-left for 5% AM at 60 Hz and carrier 8.5 MV/m gradient.

### *LFD Instability Analysis & Simulations*

Two explanations are being considered. (1) The power divider does not isolate CAV#1 from reverse power from CAV#2, and visa versa. This unintended feedback, along with the quasi-static tuning response and LLRF control loops may, alone, be sufficient cause. (2) LFD Coupling of the cavities to mechanical modes. Preliminary Routh-Hurwitz analysis [29] of (1) indicates stability in the absence of the power divider F/B path. Preliminary time domain simulation [30] of (2) in the absence of the PD F/B shows thresholding and sensitivity to the cavity static detuning. In the simulation, the microphonic frequency is taken as a given (e.g. 120 Hz), and the cavity detunings varied. As gradient is raised, the working area of shrinks to zero indicating the threshold (Fig. 5-right).

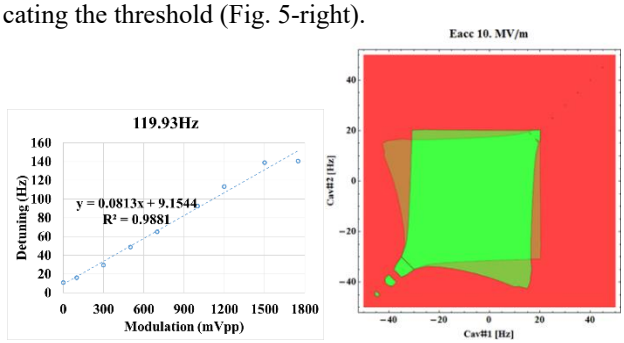


Figure 5: Left: Dynamic LFD measurement at 120 Hz. Right: Simulation output for 4 mechanical modes/cavity. Working area shrinks to 10 Hz×10 Hz at 20 MV/m.

## CONCLUSION

The magnetic optics is commissioned to 10 MeV and in excellent agreement with the theoretical model. Following the development of a new data acquisition, integration and thresholding electronic board for the BLMs, the MPS is also commissioned to 10 MeV. Troublesome microphonics effects are understood and mitigations proposed. Resolution of the ponderomotive instability through analysis, simulation and experiment will be ongoing in the spring of 2019 – when e-linac operations resume. A key will be to increase data acquisition rates from 10s to 100s of Hz.

ISBN: 978-3-95450-194-6 ISSN: 2226-0366 doi:10.18429/JACoW-LINAC2018-TU1A03

## REFERENCES


[1] S. Koscielniak, *et al*., "Proposal for a ½ MW Electron Linac for Rare Isotope and Materials Science", in *Proc. 11th European Particle Accelerator Conf. (EPAC'08)*, Genoa, Italy, Jun. 2008, paper TUOCG03, p. 985.

[2] Dilling, *et al*., "ISAC and ARIEL: The TRIUMF Radioactive Beam Facilities and the Scientific Program", Hyperfine Interactions, January 2014, Volume 225, Issue 1.

[3] J. Bagger, *et al*., "TRIUMF IN THE ARIEL ERA", in *Proc. IPAC'18*, Vancouver, Canada, Apr-May 2018, p. 6. doi:10.18429/JACoW-IPAC2018-PAMOXGB2

[4] L. Merminga, *et al*., "ARIEL: TRIUMF's Advanced Rare Isotope Laboratory", in *Proc. IPAC'11*, San Sebastian, Spain, Sep. 2011, paper WEOBA0, p. 1917.

[5] S. Koscielniak, *et al*., "ARIEL Superconducting Electron Linac", in *Proc. 26th Linear Accelerator Conf. (LINAC'12)*, Tel Aviv, Israel, Sep. 2012, paper WE1A04, p. 729.

[6] R. Laxdal, *et al*., "TRIUMF/VECC E-linac Injector Beam Test", in *Proc. 26th Linear Accelerator Conf. (LINAC'12)*, Tel Aviv, Israel, Sep. 2012, paper MOPB026, p. 231.

[7] T. Planche, *et al*., "Commissioning and Early Operation of the ARIEL E-linac", in *Proc. LINAC'16*, East Lansing, MI, USA, Sep. 2016, pp. 12-16. doi:10.18429/JACoW-LINAC16-MO2A03

[8] M. Marchetto, *et al*., "Commissioning and Operation of the ARIEL Electron Linac at TRIUMF", in *Proc. IPAC'15*, Richmond, USA, May 2015, paper WEYC3, p. 2444.

[9] R. Laxdal, *et al*., "Status of Superconducting Electron Linac Driver for Rare Ion Beam Production at TRIUMF", in *Proc. LINAC'14*, Geneva, Switzerland, Aug.-Sep. 2014, paper MOIOC01, pp. 31-35.

[10] S. Koscielniak, *et al*., "TRIUMF ARIEL e-Linac Ready for 30 MeV", in *Proc. 8th Int. Particle Accelerator Conf. (IPAC'17)*, Copenhagen, Denmark, May 2017, pp. 1361-1364. doi:10.18429/JACoW-IPAC2017-TUPAB022

[11] R. Laxdal, *et al*., "The 30 MeV stage of the ARIEL E-linac", in *Proc. 18th Int. Conf. RF Superconductivity (SRF'17)*, Lanzhou, China, Jul. 2017, pp. 6-12. doi:10.18429/JACoW-SRF2017-MOXA03

[12] Y. Ma, *et al*., "First RF Test Results of Two-Cavity Accelerator Cryomodule for ARIEL E-Linac at TRIUMF", in *Proc. IPAC'18*, Vancouver, Canada, Apr-May 2018, p. 4512-4515. doi:10.18429/JACoW-IPAC2018-THPMK090

[13] K. Fong, *et al*., "Tuners Alignment on Two 9-cell Cavities with Single Amplifier Under Self-Excited Loop", in *Proc. IPAC'18*, Vancouver, Canada, Apr-May 2018, p. 4527-4529. doi:10.18429/JACoW-IPAC2018-THPMK096

[14] F. Ames, *et al*., "Operation of an RF Modulated Thermionic Electron Source at TRIUMF", in *Proc. IPAC'18*, Vancouver, Canada, Apr-May 2018, p. 4705-4707. doi:10.18429/JACoW-IPAC2018-THPML025.

[15] F. Ames, "Commissioning Report for the TRIUMF ARIEL 300 keV electron source", TRIUMF Document -144733

[16] Y.C. Chao, "E-Linac Major Components and Layout up to Exit of Injector Cryomodule" TRIUMF internal report TRI-DN-10-08.

[17] Y.C. Chao, "E Linac EMBT-EABT-EHAT Phase One Major Components and Layout", TRIUMF report TRI-DN-12-03.

[18] Y.N. Rao, "Electron High Energy Dump Transport (EHDT) Optics Design", TRIUMF internal report TRI-DN-12-11.

[19] S. Koscielniak, "Preliminary Design of Target/Cooling Plate and Raster Pattern for a 100kW Electron Beam Dump (EBP) at 25-75 MeV", TRIUMF internal report TRI-DN-13-03.

[20] I. Earle, "E-Linac 100kW Beam Dump Insert Design Review", TRIUMF internal report DR.P0104-24.

[21] M. Alcorta, *et al*., "Status of the Machine Protection System for ARIEL E-linac", in *Proc. IPAC'18*, Vancouver, Canada, Apr-May 2018, p. 4829-4831. doi:10.18429/JACoW-IPAC2018-THPML077

[22] H. Hui, *et al*., "The TRIUMF Beam Loss Monitor Board for ARIEL", in preparation, 2018.

[23] D. Storey, *et al*., "Performance of OTR and Scintillator View Screens for the ARIEL Electron Linac", in *Proc. 8th Int. Particle Accelerator Conf. (IPAC'17)*, Copenhagen, Denmark, May 2017, pp. 117-119. doi:10.18429/JACoW-IPAC2017-MOPAB021

[24] D. Schulz, "Ponderomotive Stability of RF Resonators and Resonator Control Systems", ANL internal report, ANL-TRANS-944.

[25] J. Delayen, "Phase and Amplitude Stabilization of Superconducting Resonators", California Institute of Technology Thesis, 1978.

[26] N. Muller, *et al*., "TRIUMF's Injector and Accelerator Cryomodules", in *Proc. 17th Int. Conf. RF Superconductivity (SRF'15)*, Whistler, Canada, Sep. 2015, paper THPB115, pp. 1409-1412.

[27] Y. Ma, *et al*., "Microphonics Investigation of ARIEL E-Linac Cryomodules", the presented at the 29th Linear Accelerator Conf. (LINAC'18), Beijing, China, Sep. 2018, paper TUPO020, this conference.

[28] C. Schmidt, "Concept of Vector-Sum Control for cw-Operation", in Proc. ERL07, Daresbury UK, p. 80-84.

[29] Shane Koscielniak, personal communication.

[30] Zhongyuan Yao, personal communication.